Impact de l'écoulement interne sur le dépôt de particules dans une goutte sessile chauffée localement.

Impact of internal flow on particle deposition in a locally heated sessile droplet

Mebrouk AIT SAADA[1*], Salah CHIKH[1], Lounès TADRIST[2]

[1]USTHB, Faculté de Génie Mécanique et de Génie des Procédés, LTPMP, Alger 16111, Algérie
[2]Aix-Marseille Université, CNRS, Laboratoire IUSTI, UMR 7343, Marseille 13453, France
[*](Corresponding author: m_aitsaada@yahoo.fr)

Résumé - Cette étude numérique analyse l'impact de l'écoulement interne sur le dépôt de particules dans une goutte sessile en évaporation. La goutte colloïdale s'évapore sur une surface adiabatique et elle est chauffée localement par le dessous, soit au centre, soit à la périphérie. Le modèle numérique prend en compte les effets de la poussée, du refroidissement par évaporation et de la thermo-capillarité. Sur une surface totalement adiabatique, un écoulement dans le sens horaire, combiné à un écoulement radial sortant, entraîne un dépôt en forme d'anneau. Une surface totalement isotherme génère un écoulement dans le sens antihoraire, formant une bosse centrale. Le chauffage local périphérique crée un anneau et une bosse centrale, tandis que le chauffage local central réduit l'anneau et produit une bosse plus fine et plus étendue. Ces résultats soulignent l'influence du chauffage local sur l'écoulement interne et par conséquent sur les motifs de dépôt.

Abstract - This numerical study investigates the impact of internal flow on particle deposition in an evaporating sessile droplet. The colloidal droplet evaporates on an adiabatic surface and is locally heated from below, either at the center or the periphery. The numerical model incorporates the effects of buoyancy, evaporative cooling and thermo-capillarity. On a fully adiabatic surface, a clockwise flow combined with outward radial flow at low contact angles results in ring-shaped deposition. In contrast, a fully isothermal surface induces a counterclockwise flow, forming a central bump. Peripheral local heating enhances edge deposition, creating both a ring and a central bump. Central local heating reduces the edge ring and produces a thinner and more extended central bump. These results highlight the influence of thermal boundary conditions on internal flow and consequently on deposition patterns.

Nomenclature

C	concentration, kg/m^3
D	vapor diffusion coefficient, m^2/s
D_p	particle diffusion coefficient, m^2/s
k	thermal conductivity, W/m K
P	pressure, Pa
R	contact radius, m
T	temperature, °C
t	time, s
$\vec{V}$	velocity vector, m/s
$\vec{V}_I$	velocity vector of moving interface, m/s
$\vec{n}, \vec{t}$	normal and tangential unit vectors
X_p	particle concentration, kg/m^3
X_{ps}	particle Surface concentration, kg/m^2
Greek Symbols	
α, β, ϕ	toroidal coordinates, rd
α_T	thermal diffusivity, m^2/s
μ	dynamic viscosity, kg/m s
ρ	density, kg/m^3
$\bar{\bar{\tau}}$	stress tensor, Pa
θ	contact angle, °
σ	surface tension, N/m
Subscripts	
ℓ, g	liquid, gas
∞	at infinity in surrounding air

https://doi.org/10.25855/SFT2025-151

1. Introduction

The evaporation of sessile droplets is a complex physical process involving fluid flow, heat and mass transfer and interactions between solid, liquid and gas phases. Growing interest in this phenomenon stems from its importance in numerous technological applications. In fields such as nano-coating, chip manufacturing and disease diagnostics, precise control over the size and shape of particle deposition is a critical factor for optimizing performance [1].

The literature shows few numerical studies on particle deposition, while experimental research focuses on identifying deposition patterns and understanding their formation mechanisms [2]. Particle-substrate interaction has a minor role, while internal fluid flow in the evaporating droplet strongly influences deposition [3]. Thermal boundary conditions affect flow structure: high thermal conductivity substrates drive strong flow through thermocapillary forces and evaporation near the contact line [4, 5], while insulating substrates reduce evaporation and weaken the flow [6]. Deegan et al. [7] showed that a pinned contact line and high evaporation flux generate a radial outward flow, forming the coffee-ring stain. Gleason et al. [8] found that lower contact angles reduce radial flow, minimizing the coffee-ring effect. Yen et al. [9] used a laser-induced differential evaporation technique to create a central-peak deposition pattern by inducing a radial inward flow. Hu and Larson [10] found that the thermocapillary effect creates a cellular flow, forming a central bump-shaped deposition. Ristenpart et al. [11] showed that internal thermocapillary flow direction depends on the thermal conductivity ratio between the substrate and droplet. Malinowski et al. [12] used external vapor sources to create temperature gradients, altering internal flow and reducing the coffee-ring effect. All these results underline the importance of understanding the mechanisms driving the internal flow and the influence on particle deposition. By elucidating how thermal properties and flow dynamics interact during droplet evaporation, one can better control the size and shape of particle deposits, a key factor for applications involving colloidal droplets on homogeneous substrates.

This study investigates the evaporation of a colloidal sessile droplet through the implementation of a numerical model that accounts for both buoyancy-induced convection in the surrounding air and thermo-capillary convection within the fluid phases. The main focus is on understanding how the internal flow within the evaporating droplet influences particle transport and the resulting deposition pattern. The flow is induced by non-uniform thermal boundary conditions at the contact surface of the droplet. Specifically, a local heating is applied either at the center of the droplet or at the periphery, while the remaining surface is adiabatic.

2. Mathematical formulation

Figure 1 represents a sessile droplet with an initial volume of 1 mm^3. The liquid in the droplet is a colloidal suspension composed of polystyrene nanoparticles with a diameter of 100 nm. diluted in water with an initial concentration of 0.1 g/L (polystyrene/water density ratio ≈ 1. mass diffusion coefficient = 1.7×10^{-11} m^2/s). The droplet evaporates on a horizontal adiabatic solid surface with a radius of R_∞=100 R and an initial contact angle θ_0=50°. Local heating is applied beneath the droplet, either at its center or near its periphery. It is represented as a narrow isothermal zone with a thickness of 0.05 R and a temperature $T_w \geq T_\infty$. The spherical cap shape of the droplet and the pinned contact line are maintained during evaporation [6]. The relative humidity (Ha) is 50% and the ambient air temperature (T_∞) is 25°C.

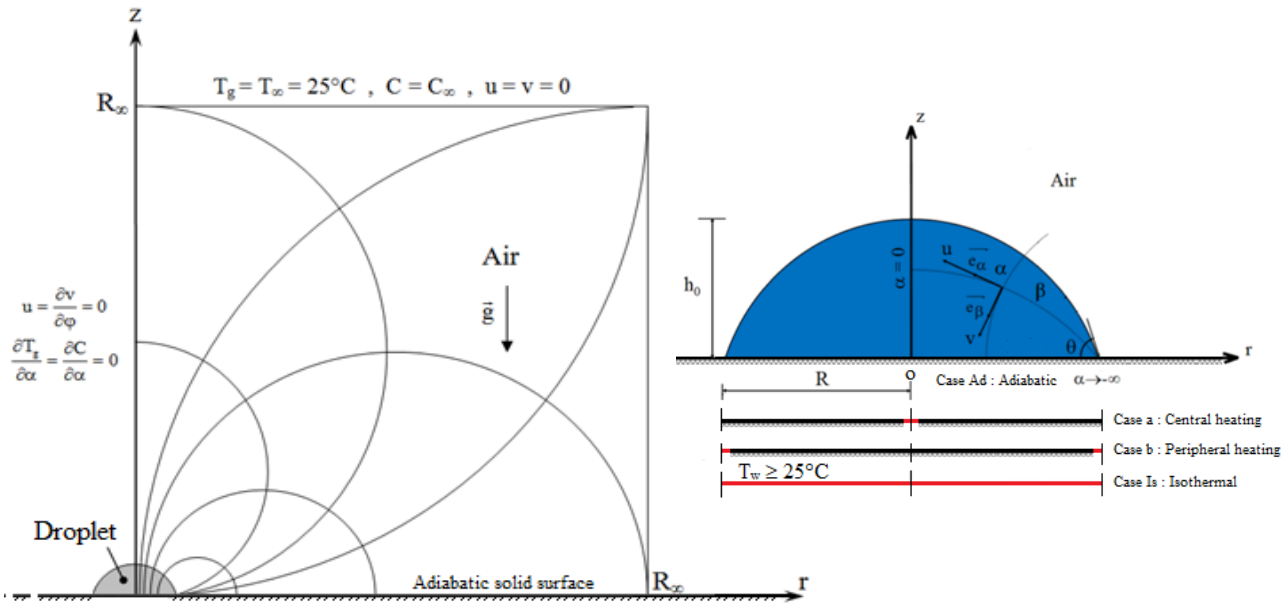

Figure 1: *Physical domain: The droplet is deposited on an adiabatic solid surface with an isothermal zone (red) located either at the droplet center (case a) or periphery (case b).*

The mathematical formulation of the studied problem is based on the continuity equation, the Navier-Stokes equations, the energy equation, the particle concentration equation within the droplet, and the vapor concentration equation in the surrounding air. These governing equations are expressed in toroidal coordinates to accurately model the interactions at the liquid-gas interface [4]. They are given by:

$$\vec{\nabla} \cdot \vec{V} = 0 \tag{1}$$

$$\rho\left(\vec{V} \cdot \vec{\nabla}\right)\vec{V} = -\vec{\nabla}P + \mu\,\Delta\vec{V} - \rho\, g\,[\beta_T(T - T_\infty) + \gamma\,\beta_C(C - C_\infty)]\,\vec{I} \tag{2}$$

$$\vec{V} \cdot \vec{\nabla}T = \alpha_T \Delta T \tag{3}$$

$$\vec{V} \cdot \vec{\nabla}C = D\,\Delta C \tag{4}$$

$$\frac{\partial X_p}{\partial t} + \vec{\nabla}.\left(\vec{V}\,X_p - D_p\,\vec{\nabla}X_p\right) = 0 \tag{5}$$

where $\beta_{T,C}$ denotes the thermal or solutal expansion coefficient of the fluid, $\vec{I}$ is a unit vector such as $\vec{I} = -\vec{e}_z$ and the parameter γ is equal to 1 in gas phase and 0 in liquid phase. For momentum, energy, and vapor mass transport, the ratio of the diffusion time (t_d) to the droplet evaporation time (t_f) is much smaller than unity. This validates the quasi-steady evolution of fields during the evaporation process. However, particle diffusion within the droplet is exceedingly slow. Consequently, the particle concentration field (X_p) evolves in an unsteady manner as the liquid-gas interface recedes. To solve the governing equations, appropriate boundary conditions must be defined. Far from the droplet, the fluid is assumed to be stationary, and the vapor concentration is given by $Ha\ C_v(T_\infty)$. The solid surface is modeled with no vapor permeability, no particle-substrate interaction, and a no-slip condition. Figure 1 illustrates the application of non-uniform thermal boundary conditions at the droplet base. At the liquid-gas interface, specific conditions are imposed to account for the physical processes governing evaporation and particle transport [4]. Mass continuity is given by:

$$\rho_\ell\left(\vec{V}_\ell\text{-}\vec{V}_I\right)\cdot\vec{n} = \rho_g\left(\vec{V}_g\text{-}\vec{V}_I\right)\cdot\vec{n} = \vec{J}\cdot\vec{n} \tag{6}$$

where J is the local evaporation flux. The total evaporation rate is obtained by integrating this flux over the entire interface. The mechanical stress balance, incorporating the thermo-capillary effect, is expressed as:

$$\left[(\vec{n}\,\bar{\bar{\tau}})_\ell - (\vec{n}\,\bar{\bar{\tau}})_g\right]\cdot\vec{t} = \nabla\sigma\cdot\vec{t} \tag{7}$$

The energy balance at the interface follows:

$$J\,h_{\ell g} - \vec{q}_\ell\cdot\vec{n} + \vec{q}_g\cdot\vec{n} = 0 \tag{8}$$

where $h_{\ell g}$ is the latent heat of evaporation and $\vec{q}$ is local heat flux. Air at the interface is in a saturated state; its vapor concentration depends on temperature. Finally, the condition for particle transport at the interface ensures that particles do not cross it:

$$\left[-D_p\,\vec{\nabla}X_p + \left(\vec{V} - \vec{V}_I\right)X_p\right].\vec{n} = 0 \tag{9}$$

3. Numerical Approach

The governing equations (1–5) along with the associated boundary and interface conditions are solved numerically by using the finite volume method in a Eulerian approach [15]. Staggered and non-uniform grids with 66×114 nodes (α×β) are utilized in the study domain with a very fine cell sizes (order of 10^{-6} R) around the contact line. Refining the mesh induces a maximum relative error less than 0.5% when evaluating the fields of u, v, P, T, C and X_p. The velocity-pressure coupling is addressed by SIMPLE algorithm. The unsteady particle transport equation (5) is time-discretized using a first order implicit scheme, with a time step chosen to correspond to a 0.01° change in the contact angle. This selection ensures both numerical stability and accuracy in tracking the evolution of particle concentration within the droplet. The time step is determined based on the evaporation rate and the variation in droplet volume. To discretize the convection and diffusion terms in the governing equations, the first order power law discretization scheme (PLDS) is employed. This method reduces numerical diffusion and provides a more accurate representation of convective effects, particularly at high Peclet numbers. The Gauss-Seidel method and the Thomas algorithm are combined to iteratively solve the system of discretized equations based on convergence criteria: maximum relative error on each dependent variable ≤ 0.1%, maximum residual of each conservation equation ≤ 10^{-5} and maximum allowable residual of continuity equation ≤ 10^{-8}. The developed computation program in Fortran is validated against the numerical results of Wang [16]. In his PhD thesis, this author numerically studied the effects of Marangoni flows on particle transport and deposition during droplet evaporation on a glass substrate. As shown in Fig. 2, a satisfactory qualitative agreement is observed by comparing the particle concentration field obtained by the computation program and that of Wang for θ = 20°.

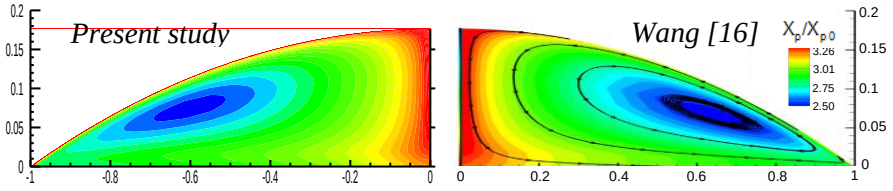

Figure 2: *Comparison with particle concentration field obtained numerically by Wang [16] for a contact angle of 20 °. The droplet is made up of water with dispersed polystyrene particles.*

4. Results and discussion

The pinned droplet evaporates on an adiabatic surface with two local heating cases: center (a) and contact line (b). Two limits are also considered: fully adiabatic (Ad) and fully isothermal

(Is). These thermal boundary conditions (BCs), applied beneath the droplet, can significantly influence internal flow patterns, thereby affecting particle transport and deposition.

Figure (3) illustrates velocity fields and temperature profiles at liquid-gas interface for a contact angle of 20°. The interface temperature gradients indicate the thermo-capillarity importance and allow to explain the flow pattern appearing inside the droplet. For the fully adiabatic contact surface (Ad), the surface temperature is low and decreases slightly from the droplet apex to the contact line, resulting in an almost negligible negative temperature gradient and very weak thermocapillary effects. This leads to a clockwise unicellular flow that transitions to an outward radial flow at low contact angles.

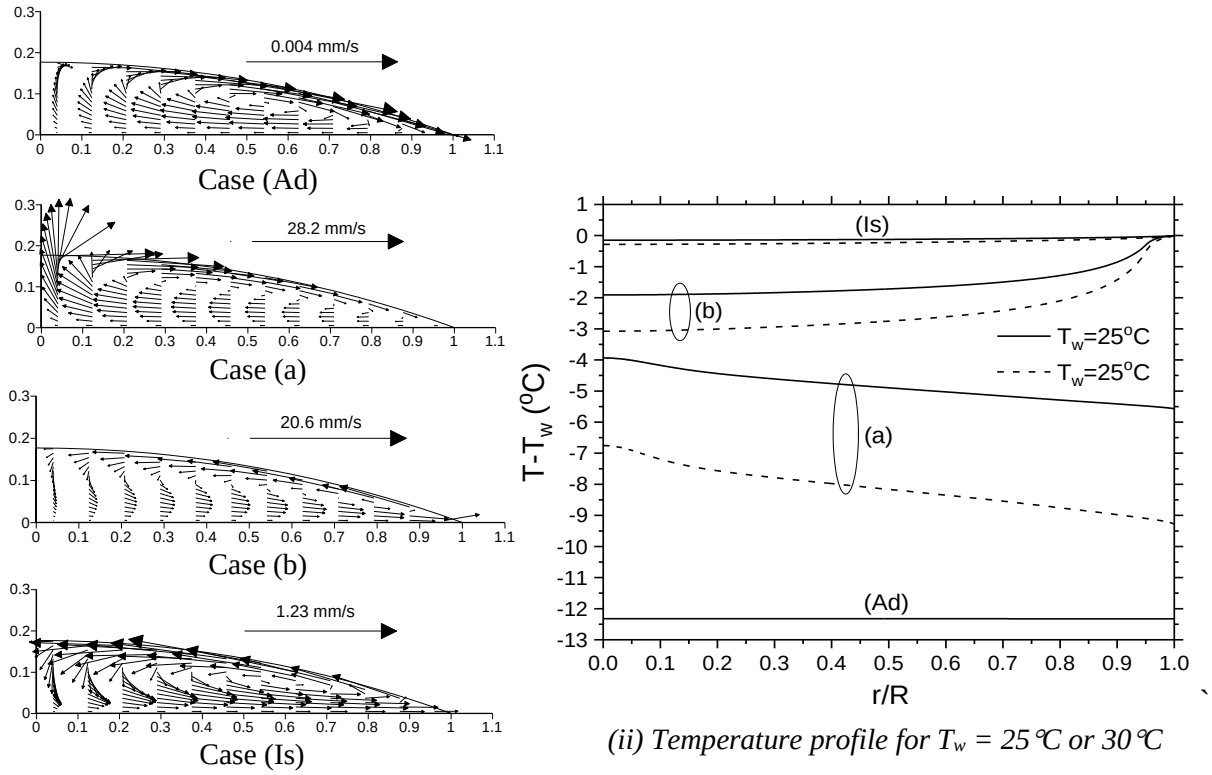

(i) Velocity field for T_w = 30℃

(ii) Temperature profile for T_w = 25℃ or 30℃

Figure 3: *Velocity fields and temperature profiles for a contact angle of 20°.*

In case (a), with local heating at the center of the wetting surface, the droplet receives more heat compared to the adiabatic case. Here, the surface temperature decreases from the apex to the contact line with a steeper gradient along the interface, generating strong thermocapillary effects that sustain a clockwise unicellular internal flow, even at low contact angles. For case (b), where local heating is applied at the contact line, the contact line temperature exceeds that of the apex. This creates significant thermocapillary effects, resulting in a counterclockwise unicellular internal flow that persists until evaporation is complete. Lastly, for the fully isothermal wetting surface (Is), the surface temperature is the highest among all cases. However, the thermocapillary effects remain weak, and the positive temperature gradient along the liquid-gas interface induces a counterclockwise unicellular flow inside the droplet.

Figure 4 shows temperature gradient variations along the liquid–gas interface as a function of the contact angle. The temperature gradient is almost zero when the drop base is subjected to fully adiabatic boundary conditions. However, it increases significantly in other cases, especially when local heating is applied with T_w = 30 °C. Thermocapillary effects are relatively weak and diminish over time as the contact angle decreases during evaporation on a fully

isothermal wetting surface. In contrast, the introduction of local heating intensifies the thermocapillary effects, which, unlike in the fully isothermal case, increase in time during evaporation. The position of the local heating significantly affects the dynamics of the cellular flow and induces its inversion. Thermocapillary effects are more pronounced when local heating is applied at the periphery of the drop (case b). However, at low contact angles, these effects become even stronger when local heating is applied at the center of the drop (case a).

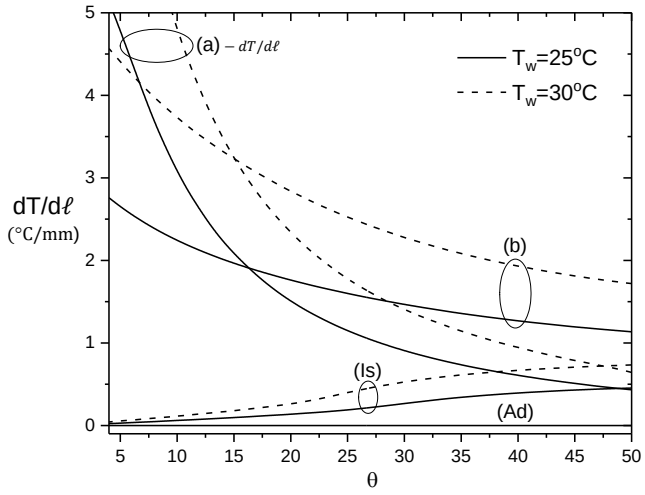

Figure 4: *Temperature gradient along liquid-gas interface as a function of contact angle.*

Figure 5 represents particle concentration fields in the sessile droplet for a wall temperature of 30°C and a contact angle of 6°. These fields are strongly influenced by the internal flow generated by the different thermal boundary conditions considered (cases Ad, a, b, Is).

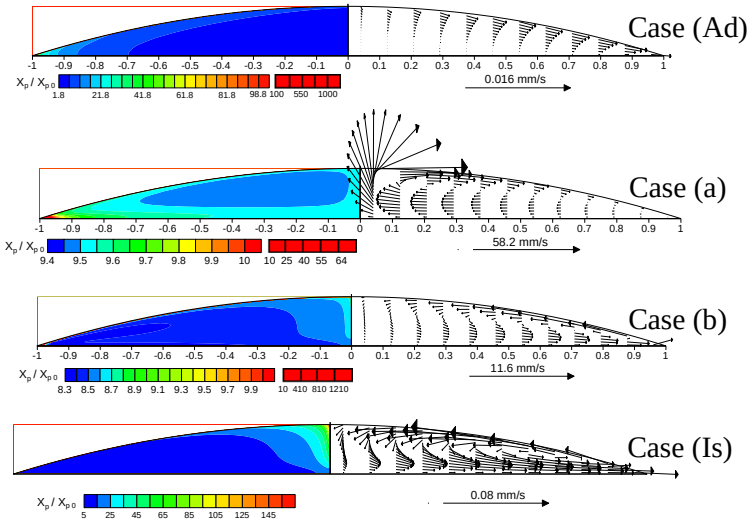

Figure 5: *Velocity fields (right) and particle concentration fields (left) for a wall temperature of 30℃ and a contact angle of 6°. At this contact angle, the droplet, due to its small volume, exhibits a significantly higher average particle concentration than the initial one.*

In the fully isothermal case (Is), particles show low concentration near the droplet edge, while they primarily accumulate in the central region. For the fully adiabatic case (Ad), thermocapillary effects induce a clockwise unicellular flow that rotates particles within the droplet. At low contact angles, such as 6°, a dominant radial flow transports particles toward the contact line, forming ring-like deposition pattern after drying. In contrast, for non-uniform thermal boundary conditions, the internal flows create distinct dynamics. In case (a), a high-velocity and clockwise unicellular flow dominates, limiting particle transport to the droplet

edge and keeping most particles circulating within the droplet. In case (b), the counterclockwise unicellular flow has a dual effect: on one hand, it transports particles toward the droplet center, and on the other, the strong evaporation around the localized isothermal zone draws particles toward the contact line. These observations demonstrate that the thermal boundary conditions at the droplet base play a crucial role in structuring the internal flows, directly influencing particle distribution and the deposition patterns formed during evaporation.

Figure 6 illustrates particle surface concentration distributions at the droplet base, evaluated near the end of evaporation at a low contact angle of 6°. The surface concentration X_{ps}, representing the mass of particles deposited per unit area, is determined without particle-substrate interaction. Below this contact angle, evaporation occurs rapidly, and the final surface concentration profile remains similar to that observed at 6°.

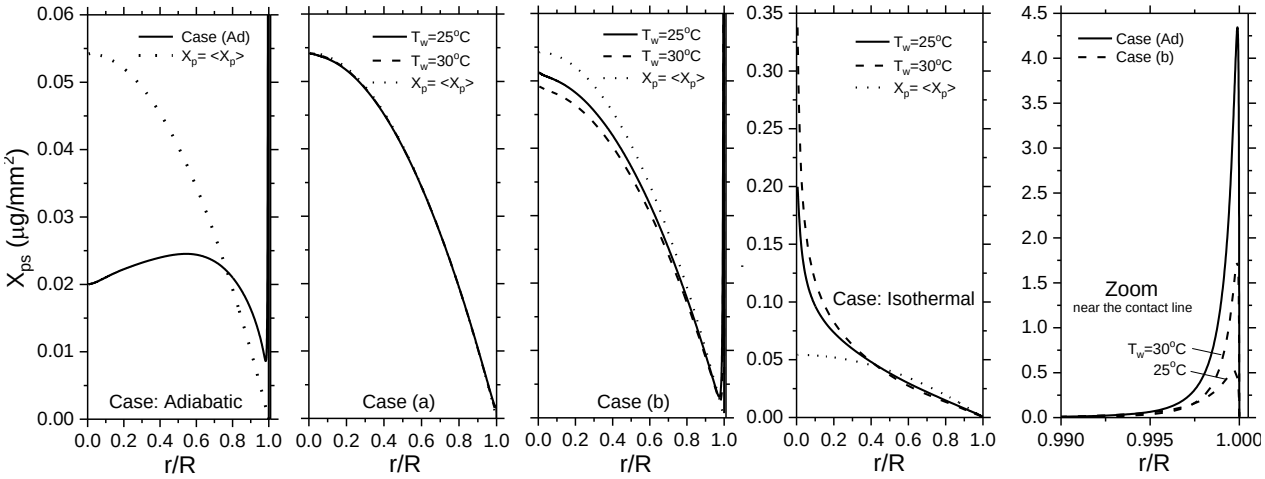

Figure 6: *Particle surface concentration profiles for a contact angle of 6° (T_w = 25°C or 30°C).*

By examining Fig. 6, distinct distributions of particle surface concentration are observed depending on the applied thermal boundary conditions. In the fully isothermal case, the maximum particle concentration is located along the central axis of the droplet, gradually decreasing to zero at the contact line. This results in particle deposition forming a bump at the center of the droplet base [10]. In the fully adiabatic case, particles form a ring of maximum concentration at the contact line, followed by a thin layer of particles spread across the rest of the wetting solid surface. In the case with a local heating at the contact line (case b), a smaller ring of particles forms near the droplet edge, compared to the fully adiabatic case. A central bump also appears, larger and thinner than in the fully isothermal case. In the case with a local heating at the center of the droplet (case a), only a few particles are transported to the contact line, forming a very small ring. Most particles recirculate inside the droplet, resulting in a wider but thinner central bump compared to the fully isothermal case [12].

5. Conclusion

A numerical investigation is conducted to study the influence of internal flow on particle deposition patterns in an evaporating sessile droplet. The colloidal suspension droplet evaporates in a pinned mode on an adiabatic solid surface with the wetting zone subjected to local isothermal heating. The numerical model incorporates the effects of buoyancy, evaporative cooling, and surface tension gradients. The results reveal that internal flow within the droplet significantly influences particle transport and deposition. For a fully adiabatic wetting surface, a clockwise unicellular flow, combined with an outward radial flow at low contact angles, leads to ring-shaped particle deposition. Conversely, for a fully isothermal

wetting surface, a counterclockwise unicellular flow during evaporation results in a central bump-shaped particle deposition. When the droplet is locally heated at the periphery of its base, strong flow near the contact line transports some particles to the droplet edge, forming a ring, while the remaining particles circulate within the droplet core, producing a central bump. However, when the droplet is locally heated at the center of its base, the ring at the edge nearly disappears and the central bump becomes more extended and thinner compared to the fully isothermal case. To conclude and provide a perspective for this work, experiments should be conducted to validate the numerical results obtained.

References

[1] M. Parsa, S. Harmand, K. Sefiane, M. Bigerelle, and R. Deltombe, Effect of Substrate Temperature on Pattern Formation of Bidispersed Particles from Volatile Drops, *J. Phys. Chem. B*, 121-48 (2017), 11002–11017.

[2] M. Ait Saada, S. Chikh, and L. Tadrist, A numerical study of particle transport in an evaporating colloidal sessile droplet, *Interfacial Phenomena and Heat Transfer*, 4-4 (2016), 217–233.

[3] D. Nagesh, P.G. Patil, R. Bange, R. Bhardwaj, and A. Sharma, Effects of Substrate Heating and Wettability on Evaporation Dynamics and Deposition Patterns for a Sessile Water Droplet Containing Colloidal Particles, *Langmuir*, 32-45 (2016), 11958–11972.

[4] C. Bouchenna, M. Ait Saada, S. Chikh, and L. Tadrist, Generalized formulation for evaporation rate and flow pattern prediction inside an evaporating pinned sessile drop, *Int. J. Heat Mass Transfer*, 109 (2017), 482–500.

[5] W. Foudhil, C. Aricò, P. Perré, and S. Ben Jabrallah, Use of Heating Configuration to Control Marangoni Circulation during Droplet Evaporation, *Water*, 14 (2022), 1653.

[6] M. Ait Saada, S. Chikh, and L. Tadrist, Evaporation of a sessile drop with pinned or receding contact line on a substrate with different thermophysical properties, *Int. J. Heat Mass Transfer*, 58 (2013), 197–208.

[7] R.D. Deegan, O. Bakajin, T.F. Dupont, G. Huber, S.R. Nagel, and T.A. Witten, Contact line deposits in an evaporating drop, *The American Physical Society*, 62 (2000), 756–765.

[8] K. Gleason, H. Voota, and S.A. Putnam, Steady-state droplet evaporation: Contact angle influence on the evaporation efficiency, *Int. J. Heat Mass Transfer*, 101 (2016), 418-426.

[9] T.M. Yen, X. Fu, T. Wei, R.U. Nayak, Y. Shi, and Y.-H. Lo, Reversing Coffee-Ring Effect by Laser-Induced Differential Evaporation, *Sci. Rep.*, 8 (2018), 1–11.

[10] H. Hu and R.G. Larson, Marangoni Effect Reverses Coffee-Ring Depositions, *J. Phys. Chem. B*, 110 (2006), 7090–7094.

[11] W.D. Ristenpart, P.G. Kim, C. Domingues, J. Wan, and H.A. Stone, Influence of substrate conductivity on circulation reversal in evaporating drops, *Phys. Rev. Lett.*, 99 (2007), 234502.

[12] R. Malinowski, G. Volpe, I.P. Parkin, and G. Volpe, Dynamic Control of Particle Deposition in Evaporating Droplets by an External Point Source of Vapor, *J. Phys. Chem. Lett.*, 3 (2018), 659–664.

[13] R.G. Larson, Transport and deposition patterns in drying sessile droplets, *AIChE J.*, 60 (2014), 1538–1571.

[14] K. Raznjevic, Handbook of thermodynamic tables, Begell House, 1995.

[15] S.V. Patankar, Numerical heat transfer and fluid flow, McGraw-Hill, Hemisphere, Washington, D.C., 1980.

[16] L. Wang, Effects of Marangoni flows on particle transport and deposition during drop evaporation, Doctoral dissertation, Purdue University, West Lafayette, Indiana, 2019.